

The low-luminosity galaxy population in the NGC 5044 Group

Sergio A. Cellone¹ and Alberto Buzzoni²

¹Facultad de Ciencias Astronómicas y Geofísicas, Universidad Nacional de La Plata, Paseo del Bosque, B1900FWA La Plata, Argentina
scellone@fcaglp.unlp.edu.ar

²INAF - Osservatorio Astronomico di Bologna, Via Ranzani 1, 40127 Bologna, Italy
buzzoni@bo.astro.it

Accepted 2004 September 21. Received 2004 September 6; in original form 2004 June 23

ABSTRACT

We present multicolour imaging for a sample of 33 dwarf and intermediate-luminosity galaxies in the field of the NGC 5044 Group, complemented with mid-resolution spectroscopy for a subsample of 13 objects. With these data, a revised membership and morphological classification is made for the galaxies in the sample. We were able to confirm all but one of the “definite members” included in the spectroscopic subsample, which were originally classified based on morphological criteria; however, an important fraction of background galaxies is probably present among “likely” and “possible” members.

The presence of a nucleus could be detected in just five out of the nine galaxies originally classified as dE,N, thus confirming the intrinsic difficulty of photographic-plate morphological classification for this kind of objects. Our deep surface photometry provided clear evidences for disc structure in at least three galaxies previously catalogued as dE or dS0. Their transition-type properties are also evident from the colour-magnitude diagram, where they lie near the late-type galaxies locus, suggesting an evolutionary connection between a parent disc-galaxy population and at least part of present-day dEs.

Half a dozen new dSph candidates were also found, most of them at small projected distances from NGC 5044, the central galaxy of the Group.

The NGC 5044 Group appears clearly defined in redshift space, with a mean heliocentric radial velocity, $\langle v_r \rangle = 2461 \pm 84 \text{ km s}^{-1}$ ($z = 0.0082$), and a moderate dispersion, $\sigma_{v_r} = 431 \text{ km s}^{-1}$. Our kinematical data show no luminosity segregation for early-type galaxies: both dwarf and bright E/S0 systems show very similar velocity distributions ($\sigma_{v_r} \sim 290 \text{ km s}^{-1}$), in contrast to late-type galaxies that seem to display a broader distribution ($\sigma_{v_r} \sim 680 \text{ km s}^{-1}$).

Key words: galaxies: NGC 5044 group – galaxies: dwarf – galaxies: photometry – galaxies: kinematics and dynamics

1 INTRODUCTION

A systematic observational work to map the low surface brightness (LSB) galaxy distribution in selected zones of the sky has been carried out by different teams, leading to complete surveys and morphological catalogues of some loose groups of galaxies and nearby clusters (Binggeli, Sandage & Tammann 1985; Karachentseva, Karachentsev & Börngen 1985; Ichikawa, Wakamatsu & Okamura 1986; Davies et al. 1988; Ferguson 1989; Ferguson & Sandage 1990; Jerjen & Dressler 1997; Secker & Harris 1997).

These catalogues serve as a basic reference to any further analysis relying on accurate photometry or spectroscopy of individual galaxies (e.g., Bothun & Mould 1988; Brodie & Huchra 1991; Cellone, Forte & Geisler 1994; Held & Mould 1994;

Secker, Harris & Plummer 1997; Cellone 1999). However, accurate observations of LSB galaxies still remain a quite difficult task both for photometry and spectroscopy, especially for clusters and groups of galaxies beyond the Virgo and Fornax Clusters. These two nearby clusters are the environments where, by far, most detailed studies of the dwarf and low-luminosity galaxy population have been carried out till present, including recent spectroscopic and photometric surveys using wide-field detectors (e.g., Hilker et al. 1999a,b; Drinkwater et al. 2000; Kambas et al. 2000; Deady et al. 2002; Sabatini et al. 2003).

A complementary view can be gained through the study of smaller groups. These have the advantage that even a moderate-sized sample would be fairly representative of the whole group population. At the same time, depth effects would be mini-

imized allowing a better analysis of distance-depending quantities. One of these rather loose groups appears surrounding the elliptical galaxy NGC 5044. The NGC 5044 Group was catalogued by Ferguson & Sandage (1990, hereafter FS90), who list 162 galaxies within ~ 45 arcmin of NGC 5044, about 80 percent of which are dwarfs ($B_T \geq 16$ mag).

Surface BV photometry for a small sample of dwarf and intermediate luminosity (mostly) elliptical galaxies in the NGC 5044 Group (of which 6 objects in common with the present work) has been presented in Cellone (1999, hereafter C99), while Khosroshahi et al. (2004) completed these results with a morphological study of a brighter sample of member galaxies, based on BRI photometry. Cellone & Buzzoni (2001) discussed the properties of a few particular dwarfs, including a possible link between dEs and blue compact dwarfs (BCD). A systematic $\text{H}\alpha$ radio survey of this field has recently been carried out by McKay et al. (2004) providing new hints for the low-surface brightness galaxy population of this loose group. In this paper we further extend the Cellone & Buzzoni (2001) analysis and present multicolour surface photometry for 33 dwarf and intermediate-luminosity galaxies (plus six likely unclassified new members) in the field of the NGC 5044 Group, along with mid-resolution spectroscopy for a subsample of 13 objects.

Our main goal is to clearly discriminate between members and background objects, in order to study (in a future paper of this series) the stellar populations and structural properties of a sample with as little background contamination as possible. At the same time, an analysis of the kinematical properties of the Group can be made.

We will arrange our discussion by presenting first, in Sec. 2, the observational input. Surface photometry for each galaxy in our sample is obtained in Sec. 3, allowing us to carry out a fully consistent morphological (re)-classification for each object and assess –in some cases with the combined help of spectroscopy– its fiducial membership to the NGC 5044 Group. Nucleated and dwarf spheroidals are reviewed in some detail in this section, and we will also present fresh data for six new galaxies, possible Group members.

The main kinematical parameters for the Group are briefly summarized in Sec. 4, while the photometric and structural properties of the full galaxy sample are dealt with in Sec. 5. Here we discuss in particular the surface-brightness vs. total magnitude relationship of the NGC 5044 members and pick up some notable candidates to transition-type objects. Given their relevance in the long-standing debate about the evolutionary connection between different dwarf-galaxy types (i.e. dE – dI – BCD), these special objects will be further characterized in Sec. 6 comparing with the global properties of the NGC 5044 galaxy population. The main issues of our discussion and our conclusions will finally be summarized in Sec. 7.

2 SAMPLE SELECTION AND OBSERVATIONS

A sample of dwarf and intermediate-luminosity galaxies was selected from the NGC 5044 Group Catalogue of FS90, with the aim of sampling most of the Group population between $15.0 \lesssim B_T \lesssim 19.0$ mag (namely, $-17 \lesssim M_B - 5 \log(h_o) \lesssim -13$ mag)¹ regardless of morphology. Galaxies classified either

¹ Throughout this paper, for the NGC 5044 Group we will adopt a distance modulus ($m - M$) = $31.96 - 5 \log(h_o)$, according to our estimate of the

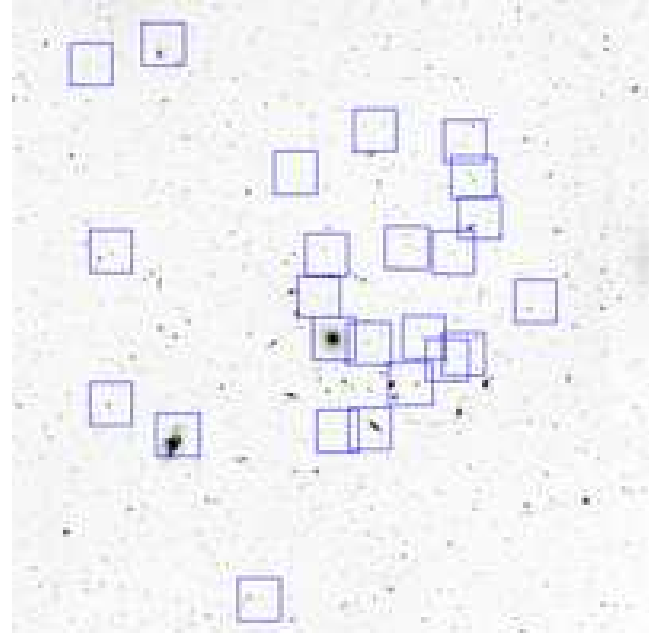


Figure 1. DSS image of the NGC 5044 Group, showing our observed fields. The frame is 90 arcmin on a side, North up, East to the left.

as definite (1), likely (2), or possible (3) members were included within our sample; only a few objects imaged with a different telescope were excluded, since those data will be presented elsewhere (Cellone & Buzzoni 2004, in preparation).

The selected fields were observed with the ESO 3.6-m telescope + EFOSC2 during two runs: April 16 – 17, 1999, and April 29 – May 1, 2000. Atmospheric conditions were photometric, with sub-arcsec seeing during the first run, while in 2000 seeing was slightly poorer ($\text{FWHM} \gtrsim 1.5$ arcsec).

2.1 Imaging

EFOSC2 was equipped with a Loral 2k CCD, which was 2×2 binned giving a scale of 0.32 arcsec pixel $^{-1}$. The instrument field thus covered an square area 5.3 arcmin on a side, allowing in most cases to image more than one galaxy within each frame. A total of 24 fields including 33 low-luminosity galaxies from FS90 (along with the bright SbI-II NGC 5054 and NGC 5044 itself) were imaged in the four bands g , r , i , z of the Gunn system (Thuan & Gunn 1976; Wade et al. 1979; Schneider, Gunn & Hoessel 1983). Individual exposure times ranged from 240 sec to 720 sec; for the faintest objects two 480 sec exposures were obtained in each band and they were summed up after all processing steps were completed. Figure 1 shows the locations of our frames on a 90×90 arcmin DSS image centred on NGC 5044.

Standard stars from the lists of Schneider et al. (1983) and Jørgensen (1994) were also observed during each run for calibration purposes.

Image processing was done using IRAF², complemented with

mean redshift for all the known group members (see Sec. 4). Note that no further correction (e.g. for the Virgocentric inflow) has been applied.

² IRAF is distributed by the National Optical Astronomy Observatories, which are operated by the Association of Universities for Research in

a few of our own FORTRAN routines. Each frame was bias corrected and then flat-fielded using twilight flats. The r and i images showed fringe patterns which had to be corrected by subtraction of the corresponding fringe image, scaled by an appropriate factor. Fringe frames were constructed by median-averaging all suited science frames in r and i , respectively; this procedure effectively removed stars and other compact objects, although the target galaxies had to be modelled and subtracted before the median-averaging could be done. We were able to satisfactorily correct fringe patterns in most of the r and i images, although rather large residuals ($\sim 1\%$ of the sky level) remained in a few images.

Cosmic rays were excised using the IRAF task COSMICRAYS. Finally, a tilted plane was fitted to the sky background and subtracted from each image.

2.2 Spectroscopy

Mid-resolution spectra were obtained for a sub-sample of 13 objects using EFOSC2 with the grism #8, in the wavelength range $\lambda\lambda 4300 - 6400 \text{ \AA}$ at 6 \AA FWHM resolution. Exposure times ranged from 1200 sec to 4800 sec, with exposures longer than 1800 sec being split into up to four shorter integrations. We used a long (~ 5 arcmin) slit, which allowed us, when possible, to include a second target galaxy on the same spectrum frame of the main object. When no catalogued galaxy could be used as second target, we tried to include any likely background galaxy within the slit; four such objects were observed in this way. A spectrum of the Group central galaxy, NGC 5044, was also obtained.

Each 2-D spectrum was bias corrected and then flat-fielded using lamp flats. One-dimensional spectra were extracted using standard routines within IRAF and wavelength-calibrated by means of He-Ne-Ar lamp spectra. Flux calibration was made with standard stars from Gutiérrez-Moreno et al. (1988), which were also observed during both runs. Finally, individual 1-D spectra of the same object were combined.

We then used the 3–8 higher S/N absorption and/or emission lines from each of our spectra to measure the corresponding radial velocities. Cross-correlation with the spectrum of NGC 5044, used as a template, provided a confirmation, and served as an initial guess for a few dubious, low S/N ratio spectra. All radial velocities given along this paper are corrected to heliocentric values.

3 MEMBERSHIP AND MORPHOLOGICAL RE-CLASSIFICATION

As usual in photographic surveys, FS90 used a morphological criterion for membership classification when redshifts were not available. This is mostly the case for dwarf ellipticals (dEs) because their low surface brightness turns them into difficult targets for spectroscopy; however, this LSB nature is in itself a very valuable tool that allows a reliable membership classification, distinguishing them from background E (i.e., high surface brightness) galaxies. Fair dEs are thus usually classified as class 1 (definite) members, while dubious objects are assigned to classes 2 (likely members) and 3 (possible members). In the Virgo and Fornax Clusters, whenever redshift information has become available for galaxies originally assigned to class 1 on morphological

bases (Binggeli et al. 1985; Ferguson 1989), membership has been confirmed for an overwhelmingly large fraction of objects (e.g., Binggeli, Popescu & Tamman 1993; Drinkwater et al. 2001), although a few striking counterexamples are widely known (e.g.: *Malin 1*, Bothun et al. 1987). On the other hand, spectroscopic surveys have also revealed a new population of compact Fornax Cluster members among objects judged as background and/or starlike on morphological bases (Hilker et al. 1999b; Phillipps et al. 2001).

Since the NGC 5044 Group is at a distance about twice that of the Virgo Cluster, it is necessary to test whether morphological membership classification still holds. Thus, our first goal was to test the FS90 membership classification for our galaxies, making a more reliable distinction between Group members and background objects. Since we have no redshift measurement for about 60% of our sample, we also had to rest on morphological criteria for these objects; however, a higher spatial resolution along with colour information allowed us to classify some dubious cases. At the same time, we were able to give a revised morphological classification for some objects.

Figure 2 shows g band contour plots for each galaxy in our sample. (“True” colour images from combined g , r , and i frames are available only in the electronic version.) For this graphical presentation, all images were sky-subtracted, median filtered and converted to the standard magnitude scale. The faintest contour corresponds to $\mu(g) = 26.5 \text{ mag arcsec}^{-2}$, with $\Delta\mu = 0.5 \text{ mag arcsec}^{-2}$ between adjacent contours. Scale is the same for all frames, which range from 1 to 3 arcmin on a side. Note the wide variety of sizes and morphologies; these will be discussed later.

From our spectroscopic data, we obtain $v_r = 2710 \pm 40 \text{ km s}^{-1}$ for NGC 5044, in coincidence with published values ($v_r = 2704 \text{ km s}^{-1}$, Huchra et al. 1983; da Costa et al. 1998). For the dwarf elliptical galaxies N42 and N50³, we confirm, within the errors, the preliminary v_r values given by C99.

Figure 3 shows the radial velocity distribution for galaxies with spectroscopic data within ~ 45 arcmin from NGC 5044; filled bars correspond to new data presented in this paper,⁴ while the empty ones show data from the literature, provided by NED. Panel *a*) spans the whole velocity range, while *b*) singles out those objects with $v_r < 8000 \text{ km s}^{-1}$.

The NGC 5044 Group appears clearly defined in redshift space, with a mean heliocentric radial velocity $\langle v_r \rangle = 2461 \pm 84 \text{ km s}^{-1}$ ($z = 0.0082$) and a moderate dispersion $\sigma_{v_r} = 431 \text{ km s}^{-1}$. A gap is evident between ~ 3500 and $\sim 5000 \text{ km s}^{-1}$. Inclusion of the four galaxies with $5400 \lesssim v_r \lesssim 6400 \text{ km s}^{-1}$ as members would raise the Group velocity dispersion to an implausibly large 1262 km s^{-1} . Three of these objects appear concentrated in the south-east quadrant of the Group, so they might belong to a background structure. In what follows, we shall thus consider all galaxies with $v_r > 3800 \text{ km s}^{-1}$ (i.e., $v_r \gtrsim \langle v_r \rangle + 3\sigma_{v_r}$) to be background objects.

Table 1 shows the results of our re-classification. Column 1 is the galaxy number in FS90, and column 2 gives our morphological re-classification. Whenever this last differed from the original one, a slanted typography was used. Column 3 gives the heliocentric radial velocity (when available); finally, column 4 gives our membership classification (question marks were used for a few dubious cases). Radial velocity uncertainties for our data in Table 1

³ In what follows, the prefix “N” stands for catalogue number in FS90

⁴ Including the dwarf N29, from Buzzoni & Cellone (2004, in preparation)

Table 1. Membership and morphological re-classification

FS90 Nr.	Morph.	v_r km s $^{-1}$	Member
Definite members ($m = 1$)			
20	dE,N		YES
30	<i>dE</i>	2411	YES
32	S0	2795 ^a	YES
34	<i>dE</i>	2661	YES
42	<i>dE/dS0</i>	2462	YES
49	ImIII	1499	YES
50	dE,N pec/BCD	2392	YES
54	dE(Huge)		YES
56	<i>dSph</i>		YES
62	<i>dSph</i>		YES
68	Sab(s)	1887 ^b	YES
70	<i>dE,N/dI</i>		YES
71	<i>d:E,N?</i>		YES
75	<i>dE</i>	1831	YES
83	<i>dE</i>		YES
84 ^c	E	2710	YES
89	dE,N		YES
109	<i>Sdm</i>	5409	NO
134	Sm(interacting)		YES
137 ^d	Sb(s)I-II(int.)	1743 ^b	YES
153	<i>d:S0</i>	2816	YES
155	Sab	2922	YES
156	<i>dE/dI</i>		YES
Likely members ($m = 2$)			
17	<i>S0pec</i>	2682	YES
24	<i>Sm</i>		NO?
55	<i>dE/dI</i>		YES
90	<i>Sc</i>		NO
138	dE,N		YES
152	<i>Sd</i>	13580	NO
Possible members ($m = 3$)			
31	<i>Im</i>		YES
33	<i>SB?c</i>	13480	NO
39	<i>E or cD</i>	27390	NO
93	bSp or Sm?		YES?
101	interacting		NO
139	<i>E</i>		NO?

a: v_r from Fairall et al. (1992)b: v_r from Huchra et al. (1983)

c: NGC 5044

d: NGC 5054

typically spanned the range $50 \text{ km s}^{-1} \lesssim \Delta v_r \lesssim 100 \text{ km s}^{-1}$, except for N109 ($\Delta v_r \simeq 250 \text{ km s}^{-1}$).

Among “definite members” ($m = 1$) with new redshift data (10 objects), only N109 ($v_r = 5409 \text{ km s}^{-1}$) lies in the near background. Classified as ImV or dE,N?, this object is in fact a late-type spiral galaxy (see Fig. 2). The remaining 9 galaxies are LSB dwarfs; their confirmation as Group members gives further support to the accuracy of morphological membership assignment for this kind of objects.

Aside from N109, no other “definite” member was reclassified as background on morphological bases. Most of these objects are dEs which can be safely considered as members. The Sm galaxy N134, in turn, is interacting with NGC 5054, and hence it must belong to the Group.

Regarding “likely” ($m = 2$) and “possible” members ($m = 3$), we present radial velocities for two objects within each class.

Figure 2. (See *fig2a.jpg* and *fig2b.jpg*.) Contour plots from *g* band images for all galaxies in the sample, in a standard magnitude scale. The faintest contour corresponds to $\mu(g) = 26.5 \text{ mag arcsec}^{-2}$, with $\Delta\mu = 0.5 \text{ mag arcsec}^{-2}$ between adjacent contours. Scale is the same for all frames, which are either 1, 2, or 3 arcmin on a side. North is up, East to the left.

Only N17 ($m = 2$) was confirmed as a Group member, although with a different morphological classification. The other three objects turned out to be in the background: N33 and N152 are late-type spirals, while N39 is a luminous elliptical ($M_V \simeq -22.3$). Judging from the “cuspy” shape of its surface brightness profile (see Sec. 5.1) N39 is probably the brightest galaxy in a background cluster (e.g., Graham et al. 1996), to which the object B1 (see Table 2) also belongs (note that object B3 is at the same redshift, however it is at $\sim 1^\circ$ projected distance from N39). Its failure as a Group member is a new confirmation of the extreme rarity of M32-type compact ellipticals (Ziegler & Bender 1998; Drinkwater et al. 2001).

Based on morphological criteria, we also reject N90, which we classify as Sc instead of dE,N (see Fig. 2; faint but well defined blue spiral arms with a few H II regions are discernible on the colour picture). The interacting pair N101 is also probably in the background, while no definite assertion can be made about the late-type spiral N24, the high surface brightness compact object N93, and the E or M32-type N139. We only retain N31 and N55 as Group members; the first one because of its resolution into star forming regions, and the second one because of its dwarf spheroidal (dSph) morphology.

As expected, all four objects included in our spectroscopy as “bonus” targets on the slit were confirmed as background galaxies (see Table 2 and Fig. 3; typical redshift uncertainties are $\Delta z \lesssim 0.001$).

3.1 Nucleated dwarfs

We observed 9 galaxies classified as dE,N (i.e., nucleated dwarf elliptical) in FS90. Despite the good seeing conditions during our observing runs, we could not detect any nucleus in N30 and N34 (see also C99); in neither case there is any luminosity enhancement in the inner regions of their surface brightness profiles (see sect. 5.1). In turn, N42 and N75 show a “cuspy” profile or bulge-type inner component, but no distinct compact central component to be regarded as a nucleus.

Hence, four out of the nine dwarfs originally classified as nucleated within our (small) sample have in fact no nucleus. Qualitatively similar results for small samples of Fornax Cluster dwarfs have been obtained previously (Cellone et al. 1994; Deady et al. 2002). In fact, Cellone et al. (1994) noted that the two largest photographic surveys in the Fornax Cluster (namely, Davies et al. 1988 and Ferguson 1989) disagree with each other in over 50% of the cases in classifying dwarf ellipticals as nucleated or non-nucleated. A high degree of coincidence is achieved, instead, between different CCD studies (e.g., Caldwell 1983; Cellone et al. 1994).

We judge this problem is a limitation inherent to photographic classification, and should be taken in mind when analysing the properties of nucleated vs. non-nucleated dwarfs, since differences between both subclasses have been reported re-

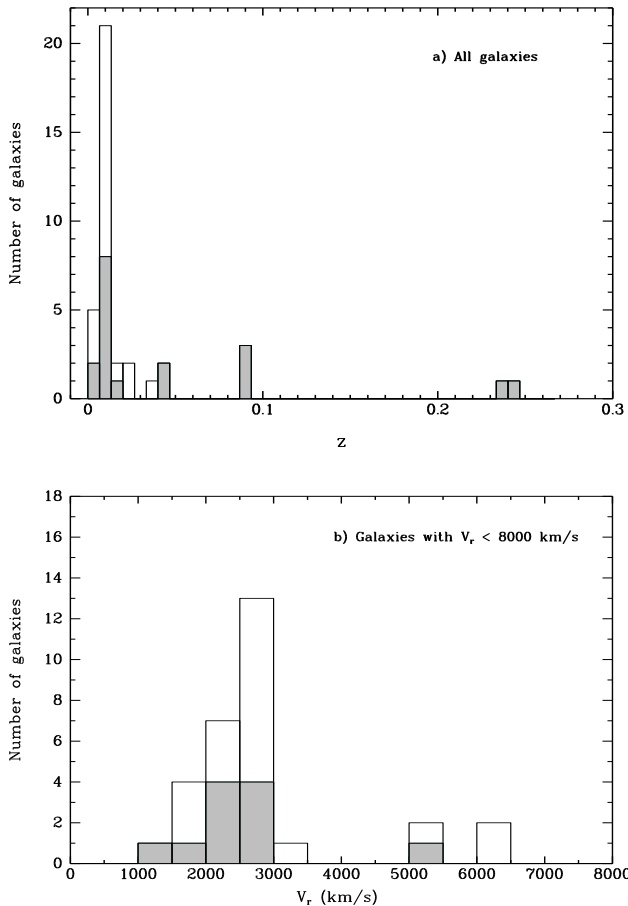


Figure 3. Radial velocity distribution for galaxies within ~ 45 arcmin from NGC 5044. Filled bars correspond to new data presented in this paper, while empty ones show data from the literature. (a) All galaxies; (b) galaxies with $v_r < 8000$ km s $^{-1}$.

garding their structure, spatial distributions, and stellar populations (e.g., Ferguson & Sandage 1989; Ryden & Terndrup 1994; Rakos & Schombert 2004). A clearer identification of nucleated dwarfs should also help to better understand their possible connection with intra-cluster globular clusters and ultra-compact dwarfs (Bassino et al. 2003; Mieske, Hilker & Infante 2004).

3.2 Candidate dSph galaxies

Six new very LSB galaxies ($\langle \mu_e \rangle(g) \sim 25.5$ mag arcsec $^{-2}$) were detected by visual inspection on our frames. Their morphologies suggest that they are previously non-catalogued NGC 5044 Group members; we named them by appending a capital letter to the name of the nearest Group member. Table 3 lists their equatorial coordinates along with our classification. Contour plots for these new galaxies are shown in Fig. 4, along with two similar objects (namely, N49A and N83A) first reported in C99 and re-imaged here.

Although we did not set any *a priori* detection criteria, a subsequent analysis shows that we were able to detect objects with isophotal g band radii (at $\mu(g) = 27$ mag arcsec $^{-2}$) larger than ~ 5 arcsec. All eight galaxies are very LSB, with central surface brightnesses fainter than ~ 24.5 mag arcsec $^{-2}$. N93A is a

Table 2. Coordinates and redshifts of background “bonus” galaxies.

Name	$\alpha_{\text{J}2000}$	$\delta_{\text{J}2000}$	z
B1	13 ^h 14 ^m 19.7 ^s	$-16^{\circ} 10' 30''$	0.097
B2	13 ^h 15 ^m 01.9 ^s	$-16^{\circ} 22' 16''$	0.282
B3	13 ^h 16 ^m 07.2 ^s	$-17^{\circ} 00' 14''$	0.096
B4	13 ^h 17 ^m 42.0 ^s	$-16^{\circ} 10' 05''$	0.277

Table 3. Coordinates and classification of new very LSB galaxies.

Name	$\alpha_{\text{J}2000}$	$\delta_{\text{J}2000}$	Morph.
N54A	13 ^h 14 ^m 42.8 ^s	$-16^{\circ} 11' 18''$	dSph
N64A	13 ^h 14 ^m 48.9 ^s	$-16^{\circ} 30' 30''$	dSph
N70A	13 ^h 14 ^m 56.7 ^s	$-15^{\circ} 52' 31''$	dSph
N93A	13 ^h 15 ^m 36.9 ^s	$-16^{\circ} 19' 22''$	dSph/dI
N93B	13 ^h 15 ^m 30.9 ^s	$-16^{\circ} 19' 22''$	dSph
N93C	13 ^h 15 ^m 35.9 ^s	$-16^{\circ} 18' 43''$	dE,N

somewhat extended object (isophotal radius $\simeq 14.5$ arcsec) with a lumpy appearance and a very shallow surface brightness profile, while N93C looks more like a faint nucleated dE.

Except for N70A ($d = 31.4$ arcmin), the new dSphs, along with the faintest catalogued dEs (N55, N56, and N62), lie within a projected distance $d = 18$ arcmin ($130 h_o^{-1}$ kpc) from NGC 5044. Furthermore, N55 and N64A are very close (a few arcmin) to the bright SBa NGC 5035; in fact, N64A was not evident until the halo of NGC 5035, as well as the wings of a saturated foreground star, were subtracted. Although the number of objects is low for statistically significant conclusions, their apparently clustered distribution would be similar to that of Local Group dSphs, which tend to be found near the Milky Way and M31. This contrasts with Kambas et al. (2000), who found a very LSB galaxy distribution in the Fornax Cluster less concentrated than the bright galaxies (but, again, see Hilker, Mieske & Infante 2003, for an opposite conclusion on the same cluster, in line with our results).

4 GROUP KINEMATICS

Table 4 shows mean heliocentric radial velocities and dispersions for the galaxies in three different morphological classes: bright early-type galaxies (E–S0), early type dwarfs (dE–dS0), and late-type objects (Sa–Im), as well as for all Group members. For ellipticals an S0s, the boundary between giants and dwarfs was set at $B_T = 15.5$ mag ($M_B = -16.5 - 5 \log(h_o)$), while the Sa–Im set encompasses both bright and dwarf objects.

Late-type galaxies seem to have a sensibly broader distribution than both dwarf and bright early-type galaxies. The intrinsically small number of members of the NGC 5044 Group prevents,

Figure 4. (See fig4.jpg.) The six new dSph candidates (plus the imaged field for galaxies N49A and N83A, already reported in C99). Each image is 1 arcmin on a side, with North up and East to the left. Contour representation is the same as for Fig. 2.

in our case, to achieve any firm quantitative conclusion in this regard; however, an *F* test on the velocity dispersion data of Table 4 confirms that late- and early-type galaxies are differently concentrated at a moderately high 93% confidence level.

Focusing on the early-type galaxies, and judging from their respective means and dispersions, it is evident that the velocity distributions of dwarf and bright objects are indistinguishable. At least for the magnitude ranges spanned by both sets, there is no hint for the luminosity segregation that shows up in the kinematic data of early-type galaxies in Virgo, which has been attributed to the merging of two sub-clumps within the Virgo core (Binggeli et al. 1993). It has also been shown that dwarf irregulars have a broader velocity distribution than bright late-type galaxies in two nearby groups (Côté et al. 1997); however, our late-type subsample is too small for further subdivision, so we cannot test this result.

Weighting the data by luminosity does not change things much, except for the fact that NGC 5044 and NGC 5054, both being ~ 1.5 mag brighter than the next brightest galaxy, tend to bias the weighted means toward higher and lower velocities, respectively. Note that the velocity of NGC 5044 is nearly 1σ larger than the Group and bright-E means; this agrees with David et al. (1994) who find evidences from X-ray data that NGC 5044 has a residual velocity with respect to the centre of the Group potential.

Our results are thus in qualitative agreement with the well known kinematical morphology segregation in clusters (e.g., Biviano et al. 2002, and references therein). Statistical studies have also found kinematical morphology segregation in groups; although there is some discrepancy regarding its significance, this seems to be mostly so for poor groups with velocity dispersions substantially lower than the NGC 5044 Group (Girardi et al. 2003; Lares, García Lambas & Sánchez 2004). On the other hand, luminosity segregation is found for galaxies ~ 3.5 mag brighter than our $B_T = 15.5$ mag giant – dwarf boundary. The lack of luminosity segregation in our early-galaxies data appears to support the Lares et al. (2004) finding that morphology (or colour index) is the primary parameter in defining dynamical properties of galaxies in groups, while luminosity segregation is mostly due to the luminosity – morphology correlation.

5 PHOTOMETRIC AND STRUCTURAL PROPERTIES

5.1 Surface brightness profiles

For each galaxy we obtained the surface brightness profile (SBP) using the IRAF task ELLIPSE. Compact foreground or background objects which could disturb the isophote-fitting algorithm were previously masked out. When necessary, the haloes of large neighbour galaxies (e.g., NGC 5035) were modelled and subtracted; the same was done with the outer wings of the PSFs of bright, saturated stars. Several non-saturated bright stars were also subtracted using DAOPHOT.

SBPs were obtained from the *g* band images, using a three-step procedure. An inner region (semi-major axis $a < a_1$) was defined as that where the error bars of the centre coordinates remained below 0.25 pixels (0.08 arcsec); within this region, all the ellipse parameters were allowed to vary freely. A second limiting semi-major axis (a_2) was set at the point where the isophote intensity dropped below a value twice its own rms; this point typically corresponds to a surface brightness $\mu(g) \approx 26$ mag arcsec $^{-2}$. For this middle region ($a_1 < a < a_2$) the centre was fixed and the fitting algorithm continued with variable ellipticity and position

Table 4. Kinematic properties.

Type	Nr.	no weights		<i>L</i> weighted	
		$\langle v_r \rangle$ km s $^{-1}$	σ_{v_r}	$\langle v_r \rangle$ km s $^{-1}$	σ_{v_r}
E-S0	9	2488 \pm 96	287	2590 \pm 87	262
dE-dS0	9	2487 \pm 98	294	2493 \pm 97	292
Sa-Im	8	2404 \pm 241	681	1982 \pm 245	693
All	26	2461 \pm 84	431	2281 \pm 98	501

angle. From a_2 outwards, all ellipse parameters remained fixed. This procedure prevented against “isophote wandering” and erratic changes in ellipticity and position angle at low surface brightness levels. However, for a few faint and/or compact galaxies, the middle region practically vanished, while for the faintest dwarfs (see Sect. 3.2) no ellipse fitting was possible at all, so we had to force fixed elliptical or circular apertures. For each object, the *g* band elliptical parameters were used to obtain the profiles in the remaining bands (*r, i, z*).

Final steps involved: a fine-tuning of the sky level (typically a few adu) by checking the flatness of the growth curve far from the galaxy centre, conversion of semi-major axis (a) to equivalent radius⁵ $\rho = \sqrt{ab}$ in arcsec, and transformation of instrumental intensities to surface brightness (μ) in standard magnitudes per square arcsec.

5.1.1 Model independent parameters

Most of our *g* band SBPs can be traced out to a surface brightness $\mu(g) \simeq 28$ mag arcsec $^{-2}$, although photometric errors get too large for intensities below one half the isophote rms, or about $\mu(g) \gtrsim 27$ mag arcsec $^{-2}$. We thus chose the $\mu(g) = 27.0$ mag arcsec $^{-2}$ isophote to measure isophotal radii (ρ_{27}), magnitudes (g_{27}), and mean surface brightnesses ($\mu_{27}(g)$). The *g* band ρ_{27} was then used to measure magnitudes and surface brightnesses in the remaining bands (*r, i, z*), so that all these parameters refer to the same physical radius.

The model independent effective radius (ρ_e) was obtained from each growth curve as the radius encompassing half the luminosity within the ρ_{27} isophote. It is clear that this is an underestimation of the actual half-light radius; however, we shall show that our isophotal magnitudes are fairly good approximations to the total brightnesses that one would obtain by integrating the observed profile to infinite radius. Consequently, the model independent effective surface brightness (μ_e) was obtained as the surface brightness at the $\rho = \rho_e$ isophote, and the mean effective surface brightness as $\langle \mu_e \rangle = g_{27} + 5 \log(\rho_e) + 1.995$.

5.1.2 SBP fitting

We fitted the *g* band SBPs with a Sérsic (1968) law: $\mu(\rho) = \mu_0 + 1.086 (\rho/\rho_o)^n$, where μ_0 is the central surface brightness, ρ_o is the pseudo scale-length, and n is the Sérsic index which governs the SBP shape. Note that we use n as the exponent in the Sérsic law, as usual for dwarf galaxies, instead of $1/n$.

It is known that fitting performances are strongly sensitive to the appropriate match of the SBP. Seeing plays an important role

⁵ We use ρ for the equivalent radius to avoid confusion with the *r* passband.

for small ρ , while noise and sky uncertainties affect on the contrary at large distances (Durrell 1997; Cellone 1999; Kelson et al. 2000). All fits were therefore carried out over a region comprised between an inner radius about twice the seeing FWHM (namely, $\rho \sim 2$ arcsec), and an outer radius assuring a sky-corrected intensity at least equal to its rms (this corresponds roughly to $\mu(g) \simeq 26.5$ mag arcsec $^{-2}$).

The flexibility of Sérsic's law allowed us to obtain satisfactory fits for most of our dwarfs, despite their very different shapes. This is true even for the few dwarfs in our sample with evidences for current star formation (N24, N31, N49).

A new set of photometric parameters, but now model dependent ones (ρ_{27}^S , g_{27}^S , $\langle \mu_e^S \rangle$, etc.), were then calculated from the Sérsic fits; when necessary, we identify them with a superscript "S" to distinguish them from their model-independent counterparts. Total magnitudes were eventually estimated by integrating the Sérsic profile: $g_T = \mu_o - 2.5 \log(2\pi\rho_o^2) - 2.5 \log[\Gamma(2/n)/n]$. Table 5 lists the relevant photometric parameters for galaxies in our sample.

5.1.3 Comparison of model-dependent vs. model-independent parameters

A check for the accuracy of the model fitting results can be made by comparing model-independent (MI) with model-dependent (MD) parameters. In general, there is a very good agreement between our MI and MD parameters, except for a few particular objects which we discuss below. Isophotal radii are slightly underestimated by the Sérsic fits ($\langle \rho_{27}^S - \rho_{27} \rangle = -0.6$ arcsec, rms = 1.6 arcsec), while the opposite is true for effective radii ($\langle \rho_e^S - \rho_e \rangle = 0.7$ arcsec, rms = 0.8 arcsec). Isophotal magnitudes and surface brightnesses show very good agreement between their MI and MD versions, with rms dispersions of 0.11 mag and 0.13 mag arcsec $^{-2}$, respectively. Slightly larger differences are obtained for mean effective surface brightnesses ($\langle \langle \mu_e^S \rangle - \langle \mu_e \rangle \rangle = 0.11$, rms = 0.16 mag arcsec $^{-2}$).

The previous results show that, in general, our fits represent a good match to the observed SBPs, and that the $\mu(g) = 27$ mag arcsec $^{-2}$ isophote is appropriate for measuring global photometric parameters. However, systematic differences are present between MI and MD parameters; they become particularly evident when comparing isophotal (g_{27}) vs. integrated (g_T) magnitudes. While the agreement is good for the brightest galaxies, fainter objects, which have larger fractions of their luminosities below $\mu(g) = 27$ mag arcsec $^{-2}$, tend to have $g_{27} - g_T > 0$. This effect can be quantified by the outer fraction of galaxy light beyond the isophotal radius, which can be defined following Trujillo, Graham & Caon (2001):

$$F(\rho_{27}^S) = \frac{L_T - L(\rho_{27}^S)}{L_T} = 1 - \frac{\gamma[2/n, b_n(\rho_{27}^S/\rho_e^S)^n]}{\Gamma(2/n)}, \quad (1)$$

where L_T and $L(\rho_{27}^S)$ are the luminosities integrated from the Sérsic law, up to infinity and up to the $\mu(g) = 27$ mag arcsec $^{-2}$ isophote, respectively, while Γ and γ are the Gamma and Incomplete-Gamma functions, respectively. Note that $\rho_e^S b_n^{-1/n} = \rho_o$, where b_n depends only on n .

In Figure 5 we plot $F(\rho_{27})$ against ρ_{27}/ρ_e^S for our galaxies (i.e., using MI values for the isophotal parameters), with filled symbols for definite members, hollow symbols for background objects, and half-filled symbols for dubious cases, and coding for different morphological types as indicated in the caption (see Table 1). Also shown are curves obtained from equation (1) for different values of n spanning the observed range. There is a clear agreement between

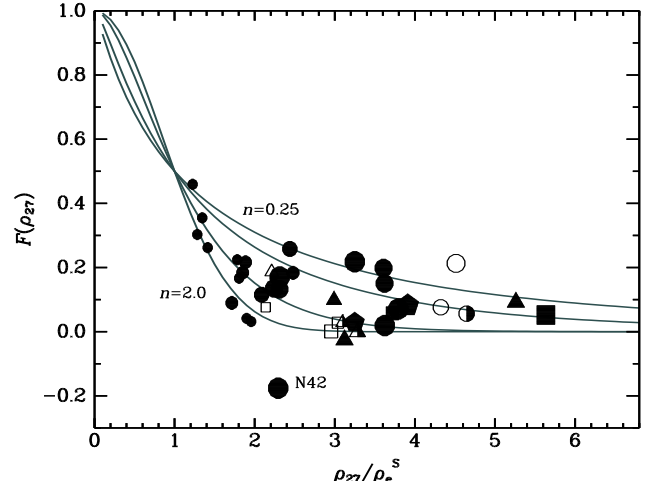


Figure 5. Fraction of galaxy light beyond the isophotal radius vs. isophotal to effective radius ratio. Circles: E-dE; pentagons: S0-dS0; squares: Sa-Sc; triangles: Sd-Im. Filled symbols: definite members; open symbols: background objects; half-filled symbols: dubious cases. Symbol sizes are proportional to integrated magnitudes. Curves obtained from equation (1) are shown for $n = 0.25$, $n = 0.4$, $n = 1$, and $n = 2$. Note the outlier object (N42 in our catalog) at $F(\rho_{27}) = -0.18$, as discussed in the text.

the observations and the expected $F(\rho_{27})$ values; in particular, the faintest, very LSB objects, have $\rho_{27}/\rho_e^S \lesssim 1.5$ and hence a large $F(\rho_{27})$. Isophotal magnitudes thus underestimate the total luminosities of the faintest galaxies by up to ~ 0.5 mag. This should be taken in mind in subsequent analyses.

In addition, a few bright members show significant differences in their MD and MI parameters. This is the case, for instance, of galaxy N42, a clear outlier in Fig. 5, with $F(\rho_{27}) = -0.18$. This dS0 galaxy consists in fact of a bulge and disc components and cannot be easily fitted by a single Sérsic law. In this case, our integrated magnitude only refers to the disc component. We will return on this object in Sec. 6.

5.2 The surface brightness – magnitude relation

Figure 6 shows the mean effective surface brightness ($\langle \mu_e \rangle$) vs. integrated magnitude (g_T) diagram for our photometric sample, with similar symbol coding as in Fig. 5. Photometry has been corrected for Galactic reddening according to Burstein & Heiles (1982).⁶ The well known magnitude – surface brightness relation is evident, with no clear segregation between early- and late-type galaxies, at least within the narrow magnitude range where there is overlap.

Confirmed and probable background galaxies occupy a differentiated region in the diagram, with a higher surface brightness for a given integrated magnitude. This corresponds to a more "spiky" apparent morphology and a lower effective radius; the $\rho_e^S = 3$ arcsec locus (dashes) is shown as a guideline. However, the distinction between members and non-members is not clear-cut; any constant radius line, within a relatively broad range, will leave

⁶ We adopted $E(B - V) = 0.03$ for the region around NGC 5044, which translates into a similar $E(g - r)$ color excess, recalling that $A(g)/E(B - V) = 3.55$ and $A(r)/E(B - V) = 2.45$ (after Scheffler 1982). For our galaxies, therefore, extinction in the g band amounts to $A(g) \sim A(V) \sim 0.11$ mag, in average.

Table 5. Observed photometric parameters

Name	ρ_{27} arcsec	ρ_e	g_{27} mag	$\mu_{27(g)}$ mag	$\langle \mu_e \rangle$ mag arcsec $^{-2}$	μ_0	ρ_0 arcsec	n	g_T mag
17	33.1	9.6	15.55	24.40	22.47	21.11	4.35	0.84	15.52
20	12.4	4.9	18.70	25.42	24.17	23.59	4.68	1.12	18.44
24	16.7	5.0	16.91	24.26	22.42	21.58	3.92	1.19	16.91
30	35.4	10.9	15.51	24.50	22.68	20.87	4.17	0.80	15.24
31	29.3	8.4	16.33	24.91	22.95	20.93	1.71	0.61	16.22
32	58.0	7.5	12.83	22.89	19.19	16.95	0.97	0.55	12.93
33	13.4	4.0	17.57	24.44	22.59	21.92	3.47	1.21	17.54
34	25.9	6.1	16.28	24.59	22.20	18.87	0.28	0.44	16.04
39	21.8	3.8	16.49	24.42	21.38	13.66	0.00028	0.22	16.23
42	44.0	13.7	15.25	24.72	22.93	22.97	14.60	1.18	15.43
49	25.3	8.2	15.75	24.01	22.33	21.58	6.96	1.30	15.78
49A	5.9	3.1	20.94	26.02	25.37
50	26.0	7.1	15.21	23.52	21.47	20.40	4.52	1.04	15.19
54	42.6	18.1	15.95	25.34	24.24	22.95	11.10	1.01	15.75
54A	5.5	3.2	21.31	26.27	25.86	25.64	4.82	1.76	20.92
55	9.4	4.4	19.64	25.74	24.83	22.76	0.98	0.61	19.18
56	13.1	6.0	18.94	25.77	24.82	24.35	6.88	1.48	18.72
62	9.5	5.0	19.80	25.93	25.29	24.79	6.43	1.26	19.13
64A	9.9	4.8	19.48	25.69	24.87	24.62	6.10	1.92	19.43
68	82.3	16.3	12.29	23.11	20.34	17.64	2.11	0.58	12.23
70	22.5	9.6	17.25	25.26	24.17	23.37	7.92	1.15	17.12
70A	7.7	4.3	20.50	26.17	25.67	25.43	6.23	1.83	20.17
71	28.0	6.8	16.43	24.90	22.60	18.78	0.17	0.40	16.25
75	29.4	6.7	15.40	23.98	21.53	22.21	9.85	1.42	15.76
83	28.9	11.0	16.70	25.25	23.90	22.75	6.38	0.92	16.55
83A	9.7	5.2	20.07	26.24	25.63	24.86	4.81	1.07	19.59
89	20.5	6.4	17.47	25.28	23.49	21.92	2.32	0.71	17.15
90	8.2	3.2	18.97	24.79	23.49	22.67	2.27	1.00	18.88
93	12.2	3.9	17.58	24.25	22.53	21.53	2.68	1.09	17.55
93A	14.5	8.0	18.91	25.97	25.42	25.14	10.60	2.16	18.81
93B	4.6	2.5	21.59	26.15	25.54	25.01	2.93	1.84	21.39
93C	8.6	4.0	19.81	25.73	24.81	24.40	4.36	1.50	19.77
109	16.1	6.5	17.66	24.95	23.72	22.57	4.09	0.96	17.44
134	36.6	5.9	15.23	24.28	21.09	19.22	1.43	0.64	15.12
138	15.4	5.2	18.15	25.33	23.72	22.39	2.49	0.82	17.93
139	15.5	3.2	17.22	24.41	21.75	19.13	0.36	0.54	17.16
152	18.2	6.1	16.72	24.26	22.64	22.14	6.46	1.62	16.72
153	46.9	11.1	14.80	24.40	22.02	19.40	1.20	0.53	14.71
155	23.4	6.2	16.19	24.28	22.17	20.52	2.28	0.79	16.13
156	31.8	13.5	16.97	25.73	24.61	23.52	9.15	1.05	16.81
B3	10.4	2.1	17.65	23.98	21.20	19.29	0.46	0.63	17.56

some members and non-members on each side. This is particularly true for N109 which, being in the near background ($v_r = 5409 \text{ km s}^{-1}$), lies intermingled with definite members in the diagram. Hence, only a coarse (statistical) membership classification can be made through the surface brightness – magnitude relation (e.g., Karick, Drinkwater & Gregg 2003).

A few galaxies scatter below the main trend. Most of these (N54, N70, N83, N156) are dEs with very shallow SBPs; they have $n \simeq 1.0$ and central surface brightnesses fainter than 23 mag arcsec $^{-2}$ in g . Galaxy N54 was originally classified as “dE(Huge)”, following the designation given by Sandage & Binggeli (1984) to large-size, LSB dwarfs found in Virgo. The other galaxies might be less extreme examples of these relatively bright but very LSB dwarfs. In turn, N156 shows an additional very interesting feature: a warped disc taking the form of a

pair of LSB outer spiral arms or tidal tails.⁷ Again, N42 lies off the main $\langle \mu_e \rangle - g_T$ relation due to its poor Sérsic fit (see also Cellone & Buzzoni 2001). We shall be back in more detail to these three notable galaxies (i.e. N54, N156 and N42) in Sec. 6.

Also shown in Fig. 6 as solid lines are the curves of constant radius ($\rho = 8 \text{ arcsec}$) at the limiting isophote ($\mu(B) = 27 \equiv \mu(g) \simeq 26.4 \text{ mag arcsec}^{-2}$) in the original catalogue of FS90, for different values of the shape parameter n . The points to the left of the $n = 1$ curve correspond to six dSph candidates discovered in the present work or in C99⁸, plus the very faint N55. Note that selection effects discriminate against faint objects with low n (i.e.,

⁷ The feature is only marginally evident from the contour map of Fig. 2 but it clearly stands out from the inspection of the original frames at the telescope.

⁸ The seventh dSph, N93A lies just rightwards the $n = 1$ curve, while the SBP of N49A has too low S/N ratio for any reliable fit to be made.

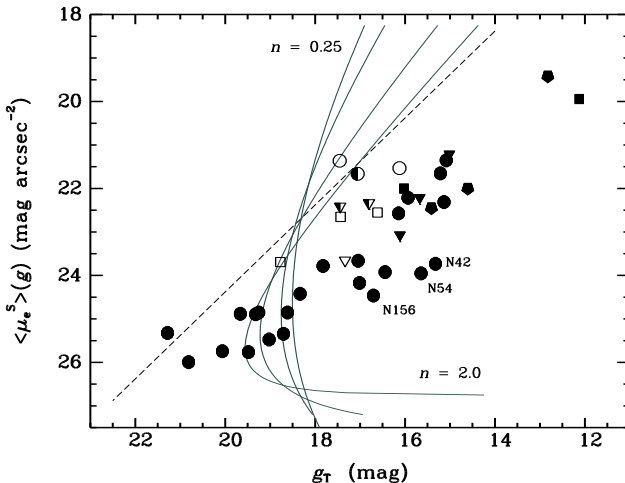


Figure 6. Mean effective surface brightness vs. integrated magnitude, both obtained from the model fits in the g Gunn band. Symbol coding is the same as for Fig. 5. Dashed line: constant effective radius, $\rho_e^S = 3$ arcsec. Solid lines: survey limits in FS90 (equivalent to $\rho = 8$ arcsec at $\mu_B = 27$ mag arcsec $^{-2}$), for $n = 0.25$, $n = 0.4$, $n = 1$, and $n = 2$. Galaxies N42, N54, and N156 (see text) are labelled. Photometry has been corrected for Galactic reddening according to Burstein & Heiles (1982).

“concave”) SBPs, an effect that might be relevant when studying the correlations of n with luminosity or size (see also Cellone et al. 1994). The existence of faint, $n < 1$ dwarfs has been confirmed from Local Group data, where selection effects of a different nature take place (Jerjen, Binggeli & Freeman 2000).

Qualitatively similar graphs are obtained by plotting any combination of surface brightness vs. magnitude, irrespective of whether they be isophotal or effective, MI or MD. However, the version used here provides the clearest member–background discrimination, and allows constant limiting radii curves to be drawn.

6 DWARFS WITH A TRANSITION-TYPE MORPHOLOGY

Since long, observational data have provided ambiguous evidence on the structure of dwarf elliptical galaxies, whether spheroidal or disky. For example, while their structureless isophotes made dEs gain their “elliptical” designation, their approximately exponential SBPs seemed to link them to disc systems. Their apparent flattening distribution, in turn, put dEs in an intermediate situation between normal E and disc galaxies (e.g. Ferguson & Binggeli 1994, and references therein).

Recently, kinematical evidence has been presented showing that at least some dEs in Virgo and the NGC 5044 Group are rotationally flattened spheroids (De Rijcke et al. 2001; Pedraz et al. 2002). The non-detection of rotation in a sample of fainter dEs, led Geha, Guhathakurta & van der Marel (2002) to suggest an association between the presence of rotation and dE luminosity. Photometric observations have also revealed “hidden” discs and/or spiral–bar features in a few dEs in Virgo (Jerjen, Kalnajs & Binggeli 2000; Barazza, Binggeli & Jerjen 2002) and Fornax (De Rijcke et al. 2003). These results seem to support models in which present-day dEs in clusters are the remnants of “harassed” disc galaxies (Moore, Lake & Katz 1998).

On the other hand, the evolutionary connection between dif-

ferent dwarf types (dE – dI – BCD) has been a subject for debate since long (e.g., Sandage & Binggeli 1984; Patterson & Thuan 1996), hence there is sustained interest in possible “transition” objects, since they may hold important keys for dwarf evolution (e.g., Vigroux et al. 1984; Sandage & Hoffman 1991; Cellone & Buzzoni 2001; Skillman et al. 2003). At least three galaxies in our sample, classified as dE or dS0 in FS90, show photometric evidence for disc structure. We describe them in the following subsections.

6.1 Warped discs in N153 and N156

N156 was originally classified as dE by FS90. As discussed in Sec. 5.2, however, the faintest ($\mu(g) \gtrsim 26$ mag arcsec $^{-2}$) isophotes in our images show an “integral sign” shape for galaxy morphology, with a warp or tidal tail emerging at each extreme of the major axis. The a_4 Fourier coefficient from the isophote-fitting routine for this galaxy is slightly negative for $\rho \gtrsim 7$ arcsec, indicating a mild boxiness for isophotes fainter than $\mu(g) \simeq 25$ mag arcsec $^{-2}$.

The low-luminosity spiral N155, a spectroscopically confirmed group member, lies at a short projected distance (1.5 arcmin $\equiv 10.7 h_o^{-1}$ kpc) from the centre of N156. It is thus tempting to invoke an interaction between both objects as the origin for the warped shape of N156. The facts that the later’s “arm” or tidal tail facing N155 points in the right direction, and that there is a hint for a counter tail at very LSB levels in N155 itself, seem to support the interaction hypothesis. Note that N155’s mean effective surface brightness is 2.5 mag arcsec $^{-2}$ brighter than that of N156, implying a higher surface mass density for the former (if similar mass to light ratios are assumed). Unfortunately, the spectrum we obtained for N156 has an insufficient S/N ratio to derive its radial velocity; hence, its kinematics with respect to N155 cannot be stated.

Sharing a similar warped appearance, N153 is however a rather different case. It was originally classified as dS0, because its disky shape is clearly seen upon visual inspection. In addition, we were able to detect a warped distortion of the outermost isophotes (see Fig. 2). These features are quantified by the a_4 coefficient, which is mildly positive (i.e., disky) within the range $10 \lesssim \rho \lesssim 20$ arcsec and definitely negative for $\rho \gtrsim 20$ arcsec, where the warping gives a boxy shape to the faintest isophotes. This trend is accompanied by a change in ellipticity, which goes from $\epsilon = 0.6$ to $\epsilon = 0.4$ over the same range in radius.

N153 is fairly isolated; it has no catalogued companion (irrespective of membership class) closer than 8.3 arcmin on the sky. One of its nearest neighbours is, remarkably, the bright spiral NGC 5054, which lies at $\sim 70 h_o^{-1}$ kpc projected distance. However, both objects differ by more than 1000 km s $^{-1}$ in radial velocity, hence an interaction is not likely.

Note that the evidences for disc structure that we found in N153 and N156 are directly observable from their images without any further processing. It is thus not unreasonable to think that more embedded disc and/or spiral features may be unveiled after appropriate image processing (e.g., Barazza et al. 2002; De Rijcke et al. 2003). A search for these kind of structures is now in progress for a larger sample of early-type dwarfs in the NGC 5044 Group (Cellone & Buzzoni 2004, in preparation).

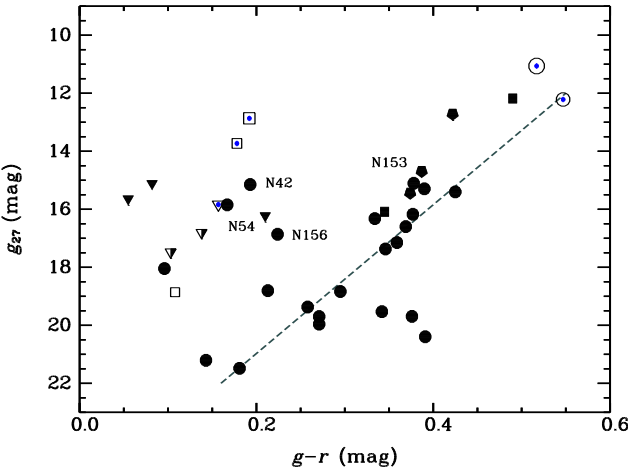


Figure 7. Isophotal colour – magnitude diagram for our sample. Symbol coding is the same as for Fig. 5, except that dotted open symbols correspond to background objects with known redshifts corrected to the distance of the NGC 5044 Group. The dashed line is the R vs. $B-R$ relation for Coma dEs from Secker et al. (1997), transformed to the Gunn system and corrected for distance. Data have been corrected for Galactic reddening according to Burstein & Heiles (1982), as explained in Sec. 5.2.

6.2 N42: a bulge plus disc system

The relevant case of N42 and its anomalous location in Fig. 5 and 6, has been extensively discussed in previous papers (C99), and especially in Cellone & Buzzoni (2001), where we showed that, although a low- n fit produces a nominally better match to the galaxy integrated magnitude, its physical sense is questionable. Our new data for N42 confirm that, trying a single Sérsic law, the resulting fit depends highly on the fitting range in ρ . With the full useful SBP we obtain $n = 0.44$, while avoiding the bulge ($\rho > 15$ arcsec) a convex shape parameter is obtained ($n = 1.18$). However, while the lower n value gives a closer match to the total luminosity of the galaxy (because it tries to include the bulge), both fits largely overestimate the effective radius of the galaxy as compared to its MI value. In addition, both high- and low- n fits make N42 drop below the main surface brightness – magnitude relation (see Sec. 5.2).

In fact, any $n < 1$ model leaves, after subtraction from the original image, both positive and negative (i.e., unphysical) significant residuals. On the other hand, $n > 1$ models give good fits to the outer region of the galaxy (the disc), leaving, after subtraction, a bulge-type component about 20% the total luminosity of the galaxy. We thus sustain a disc + bulge structure for N42, with the disc being the more luminous component. We give further support to this conclusion in the following subsection.

6.3 The colour – magnitude diagram

Although a thorough study of the evolutionary properties of the galaxies in the present sample will be presented in a forthcoming paper (Buzzoni & Cellone 2004, in preparation), it is interesting to see now whether the disc-like structural characteristics of the galaxies discussed in this section show any signature in their stellar populations.

We thus show in Fig. 7 the colour – magnitude diagram for all our sample, with the same symbol coding as in Fig. 5 and 6, except that dotted open symbols correspond to distance-corrected

magnitudes for background objects.⁹ The well known trend of redder colours (i.e., higher metallicities) for brighter systems (e.g., Caldwell 1983; Cellone et al. 1994; Secker et al. 1997; Hilker et al. 1999a) is clearly seen for the early-type galaxies. Note that, after correcting to the NGC 5044 Group distance, the two confirmed background ellipticals N39 and B3 lie not far from the extrapolation of the colour – magnitude relation for dwarfs.

Late-type objects, in turn, form a disjoint sequence with a bluer mean colour, showing no clear trend with luminosity. Note that the faintest dwarfs span a broad range in colour, which is probably due in part to large photometric errors, but may be also due to a spread in mean ages and/or metallicities. This last point is consistent with the known difficulty to distinguish between elliptical and irregular dwarfs at the faintest luminosity levels (Ferguson & Binggeli 1994).

Notably, both N42 and N156 lie on the late-type branch, as should be expected from their disc-dominated structure. The same is true for N54, a “huge” dE already mentioned because of its departure from the main trend in the surface brightness – magnitude relation (sect. 5.2). Except for the outer warped isophotes in N156, this dwarf and N54 have very similar structural properties: both are very LSB, $n = 1.0$ systems, lying well within known ranges in size, luminosity and surface brightness of dwarf irregulars (e.g., Patterson & Thuan 1996). However, there is no hint for zones of current/recent star formation in these two galaxies (neither in N42); instead, they have a very smooth appearance, which surely led to their original dE classification. Hence, we prefer an intermediate early/late type classification for them. Neutral hydrogen 21 cm observations would be highly desirable for these objects.

On the other hand, both N70 and N83, which are structurally similar to N54 and N156 (see sect. 5.2), lie on the colour – magnitude relation for early-type galaxies. Their respective locations in a two-colour diagram will give some clues on their evolutionary status (Buzzoni & Cellone 2004, in preparation)

Finally, N153 also lies on the early-type branch of the colour – magnitude relation, despite of its disk-like structure above discussed. However, its low shape parameter ($n = 0.53$) shows that, despite its detectable disc, N153 is indeed a bulge-dominated system, with its integrated red colour being the consequence of a relatively high metallicity.

7 SUMMARY AND CONCLUSIONS

In this paper we presented systematic multicolor photometry for an extended sample of 33 dwarf and intermediate-luminosity galaxies in the group of NGC 5044 (including observations for the E galaxy NGC 5044 itself, and the other luminous Sb member NGC 5054). For 13 of these objects, also mid-resolution spectroscopy was collected (this nearly doubles the galaxy sample covered in the literature for this group) in order to derive full kinematical information for each individual target and assess the dynamical status for the NGC 5044 Group as a whole.

The Group appears clearly defined in redshift space, with a mean heliocentric radial velocity, $\langle v_r \rangle = 2461 \pm 84 \text{ km s}^{-1}$ ($z = 0.0082$), and a moderate dispersion, $\sigma_{v_r} = 431 \text{ km s}^{-1}$. We

⁹ Note that, for the illustrative scope of Fig. 7, k correction has only been taken into account for background galaxies, according to Buzzoni (1995). At the distance of the NGC 5044 Group, $k \simeq 2.5 \log(1+z) \lesssim 0.01 \text{ mag}$, that is k correction is dominated by the geometrical term and is therefore negligible in our photometric bands.

also found marginal evidence of a possibly related sub-structure (at least four galaxies spectroscopically confirmed) at $v_r \sim 5000 - 6000 \text{ km s}^{-1}$, while three other galaxy aggregates seem to project on the background of the NGC 5044 field, respectively at $z = 0.045, 0.09$ and 0.28 .

Our kinematical data show no luminosity segregation among the early-type galaxy sub-samples: both the dwarf and bright E/S0 populations show nearly identical velocity distributions ($\sigma_{vr} \sim 294 \text{ km s}^{-1}$ for dwarfs and $\sigma_{vr} \sim 287 \text{ km s}^{-1}$ for bright ellipticals), while late-type galaxy distribution is on the contrary sensibly broader, with $\sigma_{vr} \sim 680 \text{ km s}^{-1}$.

On the basis of the g, r, i, z imagery, and thanks to excellent seeing conditions of our observations, we tried a revised morphological and membership classification for the galaxies in the sample. We were able to confirm all but one (i.e. galaxy N109) of the “definite members” included in the spectroscopic subsample, which were originally classified based on morphological criteria; however, an important fraction of background galaxies is probably present among “likely” and “possible” members.

The presence of a nucleus, defined as a pointlike source clearly standing out from the inwards extrapolation of the galaxy profile, could be detected in just five out of the nine galaxies originally classified as dE,N, thus confirming the intrinsic difficulty of nuclei identification on photographic plates.

Deep surface photometry down to $\mu(g) \sim 27 \text{ mag arcsec}^{-2}$ allowed us to detect six new dSph candidates (plus two other originally reported by C99, and confirmed here), most of them at small projected distances from NGC 5044, the central galaxy of the Group.

Clear evidence for disc structures in at least three galaxies previously catalogued as dE or dS0 (namely, N153, N156 and N42), was also obtained. The fact that this was inferred through different kinds of evidences, not always simultaneously present in all objects, suggests that these galaxies probably conform an heterogeneous set. It is thus necessary to extend this study, in order to shed some light on the evolutionary scenarios that led to the present-day dE population in groups. The NGC 5044 Group is particularly suited since it has about half the members as the more studied Fornax Cluster, however its central density and velocity dispersion are larger. It would be thus interesting to test whether proposed models to transform discs into spheroids, like galaxy harassment, could work in different environments.

In a second paper of this series (Buzzoni & Cellone 2004, in preparation) we will further extend our study of the NGC 5044 Group trying a more specific analysis of the distinctive properties and the evolutionary status of stellar populations in LSB galaxies of this Group.

ACKNOWLEDGMENTS

This work was based on observations collected at the European Southern Observatory, La Silla (Chile). It is a pleasure to acknowledge Michael Sterzik, Martin Kürster and the whole ESO technical staff for invaluable support during the observing runs at La Silla. We wish also to thank Michael Drinkwater, the referee of this paper, for his constructive remarks. This project received partial financial support from the Italian MIUR under COFIN'00 02-016 and CNR/GNA grants for visiting scientists. Argentinian CONICET is also acknowledged for financial support. SAC wishes to thank the kind hospitality from the Osservatorio Astronomico di

Brera (Italy), where part of this work was carried out. This work made use of the NED database supported at IPAC by NASA.

REFERENCES

Barazza F. D., Binggeli B., Jerjen H., 2002, A&A, 391, 823
 Bassino L. P., Cellone S. A., Forte J. C., Dirsch B., 2003, A&A, 399, 489
 Binggeli B., Sandage A., Tammann G. A., 1985, AJ, 90, 1681
 Binggeli B., Popescu C. C., Tammann G. A., 1993, A&AS, 98, 275
 Biviano A., Katgert P., Thomas T., Adami C., 2002, A&A, 387, 8
 Bothun G. D., Mould J. R., 1988, ApJ, 324, 123
 Bothun G. D., Impey C. D., Malin D. F., Mould J. R., 1987, AJ, 94, 23
 Brodie J. P., Huchra J. P., 1991, ApJ, 379, 157
 Burstein D., Heiles C., 1982, AJ, 87, 1165
 Buzzoni A., 1995, ApJS, 98, 69
 Caldwell N., 1983, AJ, 88, 804
 Cellone S. A., 1999, A&A, 345, 403 (C99)
 Cellone S. A., Buzzoni A., 2001, A&A, 369, 742
 Cellone S. A., Forte J. C., Geisler D., 1994, ApJS, 93, 397
 Côté S., Freeman K. C., Carignan C., Quinn P. J., 1997, AJ, 114, 1313
 da Costa L. N., et al. 1998, AJ, 116, 1
 David L. P., Jones C., Forman W., Daines S., 1994, ApJ, 428, 544
 Davies J. I., Phillipps S., Cawson M. G. M., Disney M. J., Kibblewhite E. J., 1988, MNRAS, 232, 239
 Deady J. H., Boyce P. J., Phillipps S., Drinkwater M. J., Karick A., Jones J. B., Gregg M. D., Smith R. M., 2002, MNRAS, 336, 851
 De Rijcke S., Dejonghe H., Zeilinger W. W., Hau G. K. T., 2001, ApJ, 559, L21
 De Rijcke S., Dejonghe H., Zeilinger W. W., Hau G. K. T., 2003, A&A, 400, 119
 Drinkwater M. J., et al. 2000, A&A, 355, 900
 Drinkwater M. J., Gregg M. D., Holman B. A., Brown M. J. I., 2001, MNRAS, 326, 1076
 Durrell P. R., 1997, AJ, 113, 531
 Fairall A. P., et al. 1992, AJ, 103, 11
 Ferguson H. C., 1989, AJ, 98, 367
 Ferguson H. C., Binggeli B., 1994, A&AR, 6, 67
 Ferguson H. C., Sandage A., 1989, ApJ, 346, L53
 Ferguson H. C., Sandage A., 1990, AJ, 100, 1 (FS90)
 Geha M., Guhathakurta P., van der Marel R. P., 2002, AJ, 124, 3073
 Girardi M., Rigoni E., Mardirossian F., Mezzetti M., 2003, A&A, 406, 403
 Graham A., Lauer T. R., Colless M., Postman M., 1996, ApJ, 465, 534
 Gutiérrez-Moreno A., Moreno H., Cortés G., Wenderoth E., 1988, PASP, 100, 973
 Held E. V., Mould J. R., 1994, AJ, 107, 1307
 Hilker M., Kissler-Patig M., Richtler T., Infante L., Quintana H., 1999a, A&AS, 134, 59
 Hilker M., Infante L., Vieira G., Kissler-Patig M., Richtler T., 1999b, A&AS, 134, 75
 Hilker M., Mieske S., Infante L., 2003, A&A, 397, L9
 Huchra J., Davis M., Latham D., Tonry J., 1983, ApJS, 52, 89
 Ichikawa S.-I., Wakamatsu K.-I., Okamura S., 1986, ApJS, 60, 475

Jerjen H., Dressler A., 1997, *A&AS*, 124, 1

Jerjen H., Binggeli B., Freeman K. C., 2000, *AJ*, 119, 593

Jerjen H., Kalnajs A., Binggeli B., 2000, *A&A*, 358, 845

Jørgensen I., 1994, *PASP*, 106, 967

Kambas A., Davies J. I., Smith R. M., Bianchi S., Haynes J. A., 2000, *AJ*, 120, 1316

Karachentseva V. E., Karachentsev I. D., Börngen F., 1985, *A&AS*, 60, 213

Karick A. M., Drinkwater M. J., Gregg M. D., 2003, *MNRAS*, 344, 188

Kelson D. D., Illingworth G. D., van Dokkum P. G., Franx M., 2000, *ApJ*, 531, 137

Khosroshahi H. G., Raychaudhury S., Ponman T. J., Miles T. A., Forbes D. A., 2004, *MNRAS*, 349, 527

Lares M., García Lambas D., Sánchez A. G., 2004, *MNRAS*, 352, 501

McKay N. P. F., et al. 2004, *MNRAS*, 352, 1121

Mieske S., Hilker M., Infante L., 2004, *A&A*, 418, 445

Moore B., Lake G., Katz N., 1998, *ApJ*, 495, 139

Patterson R. J., Thuan T. X., 1996, *ApJS*, 107, 103

Pedraz S., Gorgas J., Cardiel N., Sánchez-Blázquez P., Guzmán R., 2002, *MNRAS*, 332, L59

Phillipps S., Drinkwater M. J., Gregg M. D., Jones J. B., 2001, *ApJ*, 560, 201

Rakos K., Schombert J., 2004, *AJ*, 127, 1502

Ryden B. S., Terndrup D. M., 1994, *ApJ*, 425, 43

Sabatini S., Davies J., Scaramella R., Smith R., Baes M., Linder S. M., Roberts S., Testa V., 2003, *MNRAS*, 341, 981

Sandage A., Binggeli B., 1984, *AJ*, 89, 919

Sandage A., Hoffman G. L., 1991, *ApJ*, 379, L45

Scheffler H., 1982, in Landolt-Bornstein ed., Group 6, Vol. 2, *Astronomy & Astrophysics*. Springer, Berlin, p. 46

Schneider D. P., Gunn J. E., Hoessel J. G., 1983, *ApJ*, 264, 337

Secker J., Harris W. E., 1997, *PASP*, 109, 1364

Secker J., Harris W. E., Plummer J. D., 1997, *PASP*, 109, 1377

Sérsic J. L., 1968, *Atlas de galaxias australes*. Córdoba, Argentina: Observatorio Astronómico

Skillman E. D., Côté S., Miller B. W., 2003, *AJ*, 125, 593

Thuan T. X., Gunn J. E., 1976, *PASP*, 88, 543

Trujillo I., Graham A. W., Caon N., 2001, *MNRAS*, 326, 869

Vigroux L., Souviron J., Vader J. P., 1984, *A&A*, 139, L9

Wade R. A., Hoessel J. G., Elias J. H., Huchra J. P., 1979, *PASP*, 91, 35

Ziegler B. L., Bender R., 1998, *A&A*, 330, 819

This figure "fig2a.jpg" is available in "jpg" format from:

<http://arxiv.org/ps/astro-ph/0410463v1>

This figure "fig2b.jpg" is available in "jpg" format from:

<http://arxiv.org/ps/astro-ph/0410463v1>

This figure "fig4.jpg" is available in "jpg" format from:

<http://arxiv.org/ps/astro-ph/0410463v1>